Touch-at-a-Distance:
Pressure Microsensor Arrays for AUV Navigation

Sea Grant Progress Report
1 March 2008 - 28 February 2009

Sea Grant Project Number: R/RT-2/RCM-17
Grant Period: 1 March 2006 - 28 February 2012

Jeffrey H. Lang, Principal Investigator
Franz S. Hover, Co-Principal Investigator
Michael S. Triantafyllou, Co-Principal Investigator

EECS & ME Departments
Massachusetts institute of Technology
Cambridge, MA 02139

Introduction

Inspired by the lateral-line organ in fish, the ultimate objective of this project continues to be the development of a passive system for AUVs that can detect, classify and locate underwater objects. The lateral line sensory organ in fish enables some species to form three-dimensional maps of their surroundings. The canal subsystem of that organ acts as an array of pressure sensors. Interpreting spatial pressure gradients allows fish to perform a variety of actions from schooling, to tracking prey, to recognizing nearby objects. Similarly, by measuring pressure variations on a vehicle surface, an engineered dense pressure-sensor array could enable the identification and location of obstacles during navigation. Our navigation system is based upon two key technologies: (1) large arrays of very small pressure sensors that can be mounted on the surface of an AUV, and (2) the pressure signal processing algorithms through which object detection, classification and location is implemented. Correspondingly, this project is organized during its early years around the development of these two key technologies.

The development of a passive system to detect, classify and locate underwater objects will benefit AUVs that navigate cluttered environments and surf zones. Of particular importance here is the expected low power consumption of a passive system. More generally, the marine industry, especially the ROV and AUV industry, will benefit from the pressure sensing system by having available detailed flow maps derived through the pressure measurements. These maps could facilitate the optimized maneuvering and handling of turbulent flows, as well as the development of morphing procedures to reduce drag and optimize agility. Other marine industries are expected to benefit as well. For example, the oil industry could use the sensor arrays in pipelines to sense and control flow, and competitive sailing teams could use the sensor arrays to guide sail arrangements to optimize lift production, particularly during maneuvering.

Our progress made on the development of both key technologies during the past year extending from 1 March 2008 through 28 February 2009 is summarized below; progress made during earlier years is summarized in [1,2], and our Annual Reports to Sea Grant from 2007 and 2008. In general, this project is on schedule, and on budget. No significant changes to the research plan, schedule or budget need be reported at this time.

Pressure Signal Processing Algorithms

Experiments with fish provide evidence that they can extract considerable practical information about nearby objects and their surroundings from the pressure distribution along their bodies. In particular, the canal subsystem of the lateral line appears to be the critical component of many associated behaviors. Correspondingly, one of the key technologies under development here is a collection of algorithms that use the pressure field along a body to obtain detailed information about the presence, shape and location of objects in the nearby flow.

A major focus of our research during the past year has been the detection and identification of vortices. Vortices are an important class of stimuli for lateral-line-like sensors. They are of interest by themselves as persistent fluid structures that affect the performance of AUVs and their control surfaces. Frequently, they are also evidence of a nearby object interacting with the

flow. While the near-field pressure distribution resulting from the interaction between a body and flow decays fairly quickly with distance, the vortices generated by that interaction are frequently advected much further. Characteristics such as the trajectory, strength and frequency of the vortices thus also contain information about the initial object that generated them.

In order to obtain usable information from vortices in the flow, it is necessary to first detect and identify them. There is substantial evidence that the lateral line is an adequate sensor for detecting vortices. In addition to experiments with fish detecting vortices behind obstructions in streams, previous studies have indicated that pressure sensors can be used to determine the position and strength of vortices under enclosed conditions with well-characterized flow [3].

Using a two-dimensional potential flow model, vortices are fully characterized by their position and strength. In order to track these variables, an estimation algorithm based on and Extended Kalman Filter with a potential flow model has been developed and implemented. This estimator utilizes all the past pressure data to obtain an estimate of the vortex in an uncharacterized flow.

To confirm the accuracy of the estimator in tracking vortices, experiments have been conducted at the MIT Tow-Tank Facility in which an array of four pressure sensors enclosed in a streamlined housing was used to track individual vortices their its vicinity. The vortices were generated through the motion of a paddle in still water near the sensors. Figure 1 depicts the layout of the experiments. An independent estimate of the location of the vortices was obtained using concurrent particle image velocimetry (PIV) measurements.
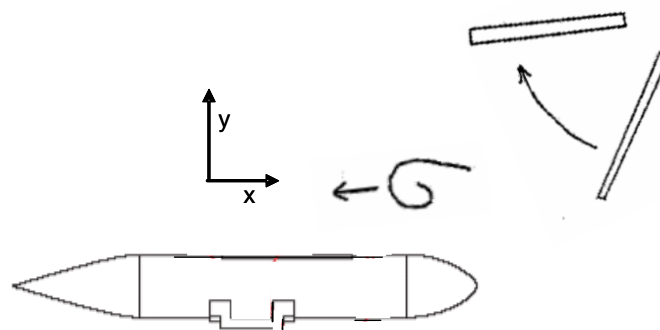

Figure 1: diagram of experimental setup. Four off-the-shelf pressure sensors are enclosed in a streamlined body to constitute the sensor array. A large paddle is used to generate a vortex in the vicinity of the pressure sensors.

The tow-tank experiments provided strong pressure signals for testing the estimator. One set of pressure signals is shown in Figure 2. A comparison between the estimated position and strength of a vortex based solely on pressure data finds that the algorithm tracks single vortices very well in the x direction along the sensor body, and slightly less well in the y direction normal to the body. It also tracks the vortex strength well. These results are illustrated in Figures 3 and 4. In summary, the estimator described above was found through the experiments to track single

vortices successfully. Currently the estimator is being extended to handle the detection and identification multiple vortices.
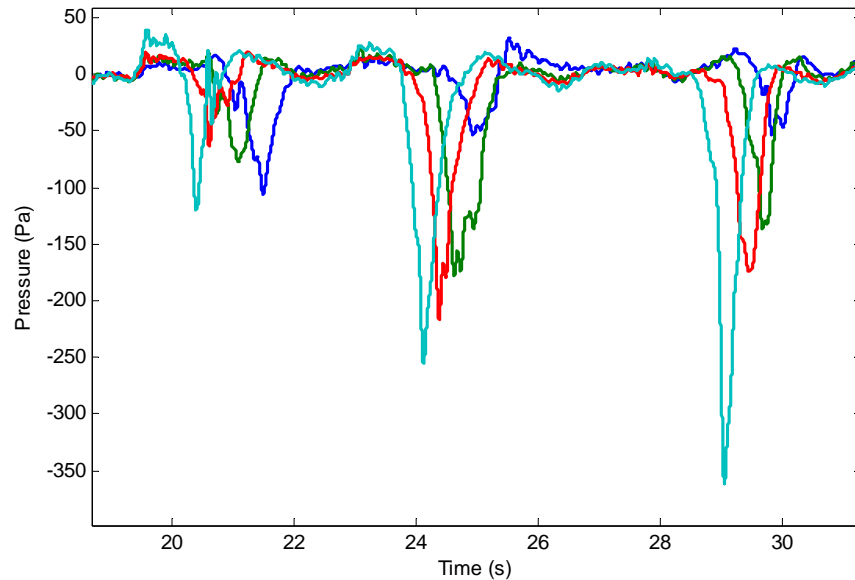

Figure 2: one set of pressure measurements from all four sensors as three vortices pass the pressure sensor array. These measurements are the basis for the vortex tracking algorithm.

The inverse problem of determining the shape of a physical object in a flow was also studied further during the past year. Previously [2], the dependence of the estimation of the shape of an object on distance and angle was studied using potential flow models of cylinders and rectangular objects. A conformal mapping generated by collaborators working under the supervision of Professor Richard Yue at MIT has provided a general method to extend our earlier work, and form the basis for parameter estimation. The mapping was applied to simulations in which a vehicle or fish swam a full circle at constant radius to probe an object in steady flow. Using a simple least squares error minimization technique, it was possible to show the convergence of the shape estimate to the actual shape as the fish swam closer to the object.
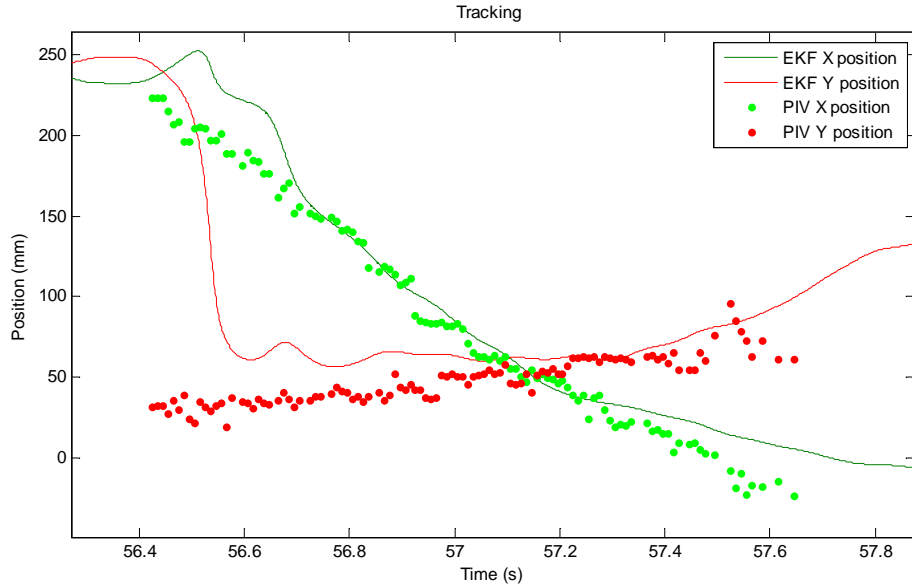
Figure 3: tracking a vortex position by pressure measurements. This figure compares the position of a vortex estimated by the tracking estimator using pressure measurements to the position found from PIV data. After an initial convergence period, the estimated position follows the observed position, with some a deviation in the perpendicular distance from the sensors.
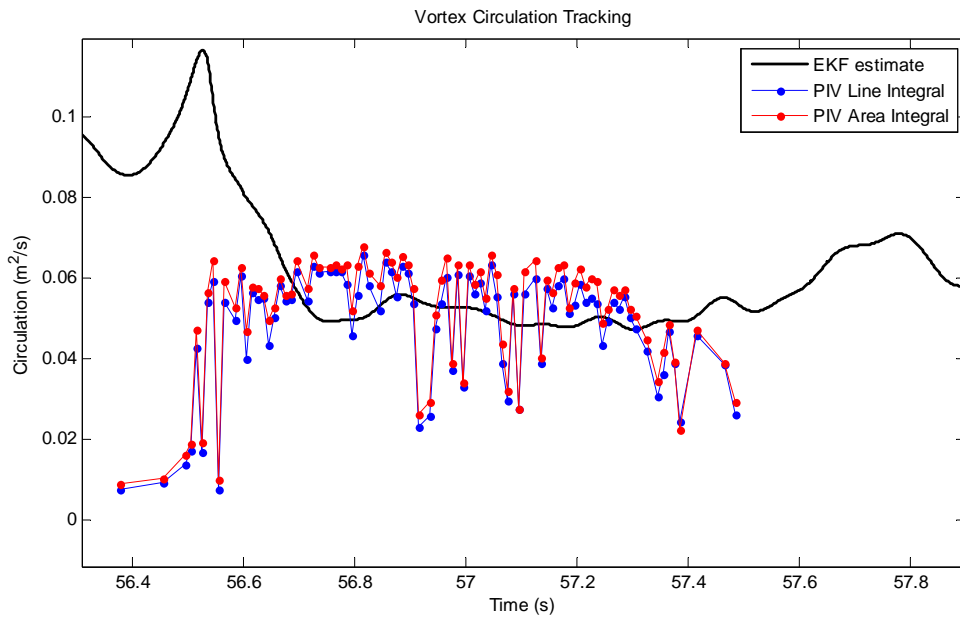

Figure 4: tracking the vortex circulation by pressure measurements. The estimate of the vortex strength corresponding to the position in Figure 3 is plotted as the solid line. For comparison, estimates of the vortex strength were calculated from the PIV using two methods. The first is a line integral to directly calculate the circulation about a closed path around the vortex center. The second is an area integral of the vorticity. Again, after an initial convergence period, the estimate and independent calculations match.

Pressure Sensor Arrays

Our development of pressure sensor arrays follows two related paths. To begin, we are implementing the pressure sensor arrays in silicon. Silicon is used here because it offers a stable and well-controlled development environment. However, for the future, we are examining the use of plastic as an alternative to silicon. It is for this reason that the pressure sensors under development do not use any of the special electrical characteristics of silicon traditionally used in pressure sensors. Plastic should be a significantly more rugged and flexible alternative. Here we are focusing initially on ABS plastic because structures of significant complexity can be fabricated from ABS plastic using three-dimensional printing. Progress along both paths is described below.

Silicon-Based Pressure Sensors and Arrays

During the past year we fabricated several wafers of pressure sensor arrays in silicon. This work follows our development of individual sensor cells during prior years [1,2]. The sensors are based on strain gauges located on the surface of deformable diaphragms that share a common internal back-side plenum; the diaphragms deform in response to local pressure. In the array wafers, the sensors are placed 2 mm apart, and the common plenum is connected to the open environment through a long winding air channel. The air channel enables the back pressure in the plenum to be equalized slowly against the large-signal pressure in the environment. In this way the pressure sensors respond to small signal pressure variations independent of depth. The target pressure resolution for a single sensor is 1 Pa, which corresponds to the noiseless disturbance created by the presence of a 0.1 m radius cylinder in a flow of 0.5 m/s at a distance of 1.5 m. A key feature of each sensor is the flexible diaphragm, which formed from a 20-μm layer of silicon attached at its edges to a silicon cavity. The strain on the diaphragm due to pressure differences across the diaphragm is measured with strain gauges, and from this strain the pressure across the diaphragm is determined. At this point in time, individual MEMS pressure sensors have been fabricated, and demonstrated to work well. In addition, arrays of pressure sensors have also been fabricated. Testing of the arrays is now underway.

The fabrication of the pressure sensors and their arrays is performed in the MIT Microsystems Technology Laboratories using standard CMOS/MEMS fabrication process steps. It is briefly described here. To begin, a double-side-polished silicon-on-insulator (SOI) wafer is first masked with a silicon-nitride layer; the wafer contains a 20-μm-thick silicon device layer which will become the diaphragm. The nitride is removed from the device (diaphragm) side, oxide is grown on the bare silicon to act as an insulating layer, and metal strain-gauge resistors are deposited on the oxide. The back side of the SOI wafer is then etched using potassium-hydroxide (KOH) with the nitride as a mask, and the original SOI oxide as an etch stop to form an air cavity. The remaining nitride mask is then dry-etched away to expose silicon. In parallel, a Pyrex glass wafer is laser etched, or wet etched in HF, to create shallow valleys that allow air to pass. The Pyrex and SOI wafers are then anodically bonded to form arrays of pressure sensors.

In one early fabrication run, a wafer set consisting of nine nearly identical columns of sensors was fabricated. The two outside columns were different from the others in that they had two fewer sensors. Otherwise, each column consisted of ten sensors; two each having diaphragm

sizes of 1 mm, 1.41 mm, 2 mm, 2.42 mm and 4 mm. The ten sensors in each column shared a single air cavity, and the ten air cavities were isolated from one another. One diaphragm from each column was broken and glued to a copper tube. A manometer was attached to the copper tube and used to control the back pressure on the corresponding column of sensors. The manometer could produce pressure differences between -1500 Pa and 1500 Pa across the pressure-sensor diaphragms with a precision of 10 Pa. Using this arrangement, the deflection away from equilibrium of the center of a diaphragm was measured as a function of pressure using a Zygo profilometer. The experimental set up is shown in Figure 5.
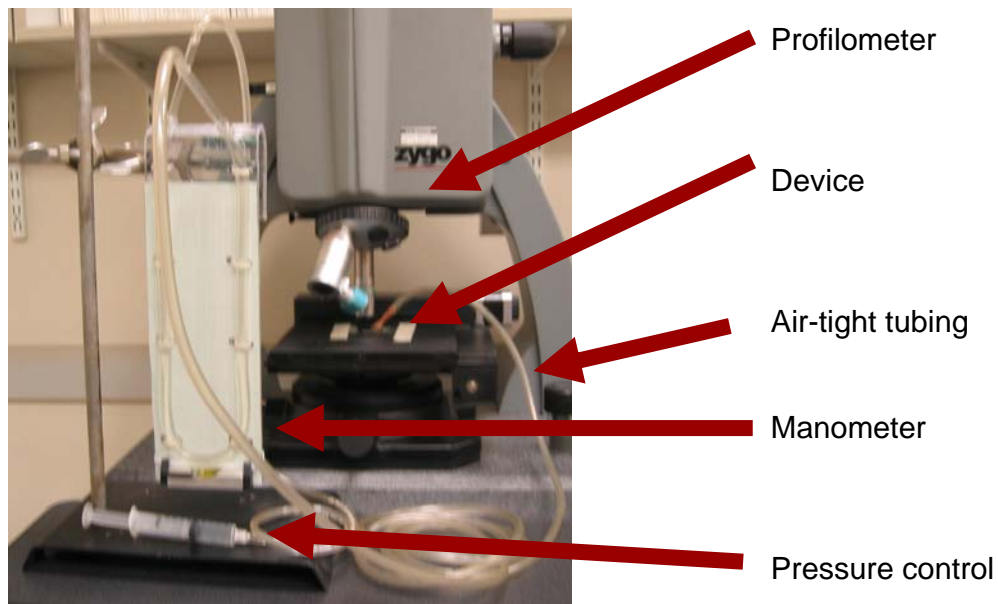

Figure 5: experimental setup for testing individual pressure sensors.

Figure 6 shows the deflection of a 2.8-mm diaphragm under 2000 Pa of negative pressure as measured with the Zygo profilometer. The color pictures in the upper left and right show the normal and oblique views of the diaphragm deflection, respectively. The green line in the picture in the lower left shows the diaphragm deflection at a central cross-section of the two-dimensional diaphragm; the cross section cut is shown in the upper left picture. The picture in the lower right is an optical view of the diaphragm. While the diaphragm is indistinguishable from the bordering silicon, the metal strain-gauge resistors on top of the diaphragm are observable. The important results from this experiment are that the membrane deflection was qualitatively as expected. Figure 7 shows the results from tests of two diaphragms of sizes 2 mm and 2.828 mm. The measured diaphragm deflections are 0.51 nm/Pa and 2.54 nm/Pa, respectively. The theoretical deflections are 1.26 nm/Pa and 5.07 nm/Pa, respectively. The difference between theory and experiment is likely the result of fabrication variations, including diaphragm pre-stress created during high-temperature oxide growth and/or metalization, and dimensional variations of the diaphragm thickness.
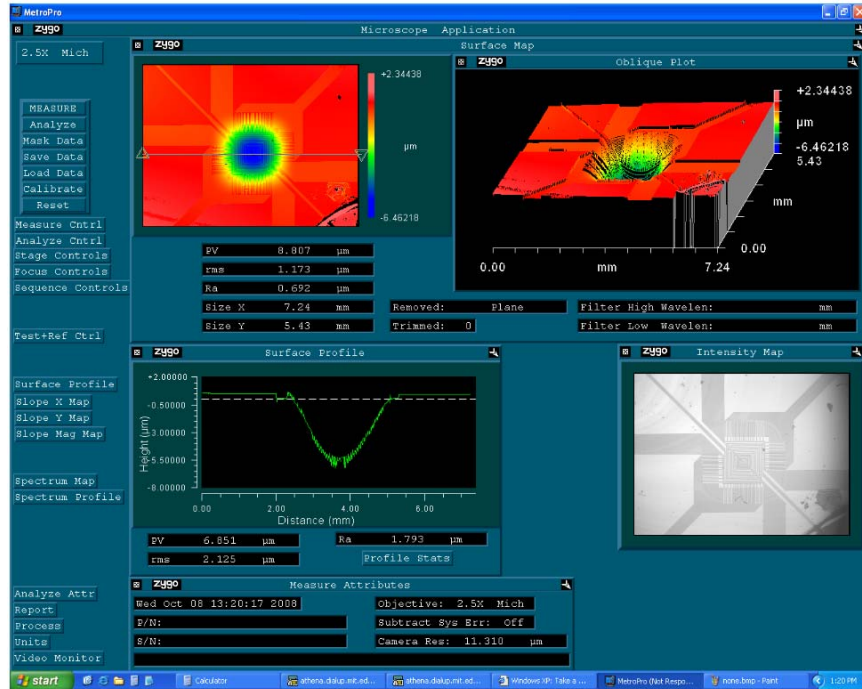
Figure 6: deflection of a 2.8 mm diaphragm under 2000 Pa of negative pressure as measured with the Zygo profilometer.
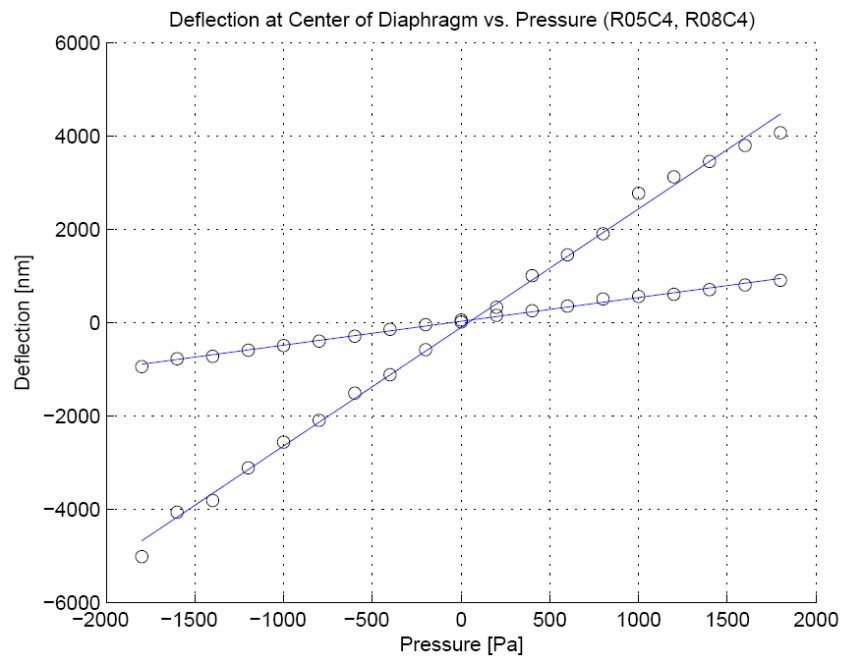

Figure 7: center deflection of a 2-mm and 2.828-mm diaphragm.

The pressure sensors have also been tested electrically as shown in Figure 8. In this experiment, one strain-gauge resistor was connected to an external bridge feeding an AD620 low-power instrumentation amplifier from Analog Devices. The amplifier was wired for a gain of 960. The output of the amplifier was read on a voltmeter and on an oscilloscope. Prior to experimentation, the bridge was tuned to produce zero output for a zero pressure difference across the diaphragm. During experimentation, the amplifier output was measured as the sensor back pressure was varied using the manometer in Figure 5. From the amplified bridge voltage, the relative change in resistance of the strain-gauge resistor, ΔR/R, was determined as a function of pressure. Figure 8 shows one such a plot for each of the four strain-gauge resistors on a selected diaphragm having a width of 2.82 mm. As expected, two of the measurements vary positively with pressure while the other two vary negatively.
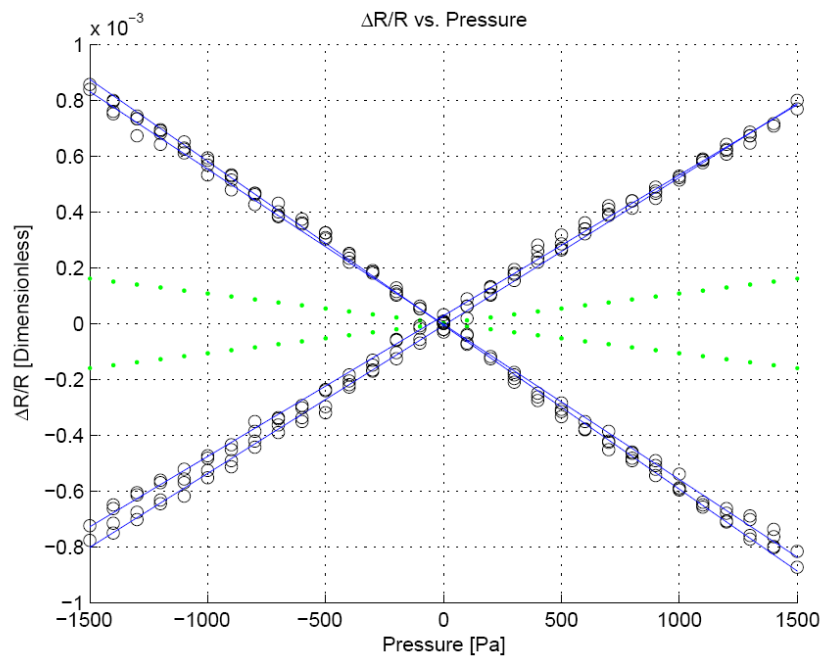

Figure 8: resistor variations from a pressure sensor.

With a diaphragm having a width of 2.82 mm, the experimental variations of (ΔR/R) were measured to be −0.294 μΩ/Ω·Pa, −0.278 μΩ/Ω·Pa, 0.252 μΩ/Ω·Pa and 0.265 μΩ/Ω·Pa. The expected theoretical values were all ±0.107 μΩ/Ω·Pa. There are several possible explanations for the discrepancy between theory and experiment. The most likely explanation is that the diaphragm, which is nominally 20 μm thick, is actually thinner than expected. SEM measurements confirm that the thickness is indeed 18.1 μm. This could be due to manufacturing variations from the vendor, or to slight over-etching from the KOH; the specifications state that the thickness is precise to within 1 μm. Since sensitivity is inversely related to the cube of the diaphragm thickness, small changes in the thickness can have a significant effect on the sensitivity. Another explanation is that the diaphragms were stretched and deformed somewhat during the fabrication process. The fabrication process has several steps in which the wafer is

placed under varying pressures from vacuum to atmospheric pressure. It was observed, for example, that the largest membranes were permanently plastically deformed. Perhaps the smaller ones were affected as well, though not to the same degree as the larger ones. In any case, the sensitivity of the sensor cells is better than expected.

In addition to the individual pressure sensors described above, arrays of pressure sensors have been fabricated. These sensors are placed much closer together (2 mm apart) and share a common winding air channel that is open to the environment. This enables the back pressure to be equalized by the large-signal pressure in the environment. The resistors are wired on-chip in a bridge configuration. Testing of the arrays is now underway.

Plastic-Based Pressure Sensors and Arrays

Acrylonitrile Butadiene Styrene (ABS) plastic has been chosen as the structural material with which to begin the development of plastic pressure sensors. ABS plastic is a strong low-mass low-loss plastic that can undergo a large strain without permanent deformation. Furthermore, complex structures can be fabricated from ABS plastic using 3D micro-printing available at MIT. In addition, it is easy to embed metal strain-gauge resistors into an ABS structure.

In order to design a pressure sensor around ABS plastic, it is necessary to know several critical mechanical properties of the plastic. These include its mass density, its Young's modulus, its Poisson's ratio, and its yield stress. Several test structures have been constructed and exercised in order to determine each of these properties. For example, Figure 9 shows a set of cantilevered beams fabricated from ABS plastic using 3D micro-printing; they are mounted on a shaker table. The beams have different lengths, different thicknesses, and different printing orientations. They are also loaded with different masses. By sweeping the frequency of the shaker table vibration, and measuring the vibration response of the beams, sufficient data is collected to determine many of the desired properties. Mass density and yield stress experiments have also been conducted. For example, Figure 10 shows a block of ABS plastic undergoing a stress-strain test in a tensometer. In addition to determining the critical material properties, it has been determined that features as small as 100 μm in every dimension can be printed using the 3D micro-printer at MIT.

ABS plastic, as manufactured by 3D micro-printing, is porous, and hence unacceptable for use in a pressure sensor. Therefore, we have determined several ways of successfully sealing ABS structures. One such process involves re-flowing the porous printed plastic using the plastic solvent Dichloromethane (DMC). Another process involves filling the pores with a paraffin solution. The effects of these sealants on the mechanical properties of the bulk material must be studied further, but upon initial investigation they appear to be minor. The DMC, being a solvent, is more difficult to control, but produces a stronger seal. The paraffin seal produces a very thin coating on the order of a few microns thick, and could possibly be used as a protective coat for the electronic sensing element.
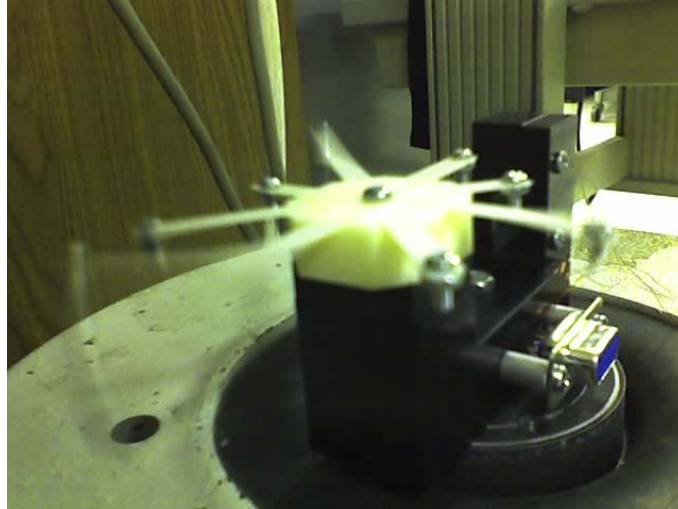
Figure 9: cantilevered beams made from ABS plastic vibrating on a shaker table.

Figure 10: a block of ABS plastic undergoing stress-strain tests in a tensometer.

Finally the surface of sealed ABS plastic is somewhat rough, too rough for the deposition of metal strain-gauge resistors. Consequently, we have also developed a suitable polishing procedure, the results of which are shown in Figure 11. The left-hand figure shows a sealed ABS plastic surface before polishing. Its roughness is several tens of microns. The right-hand figure shows a similar surface after polishing. Its roughness is only a micron or two. This is smooth enough to support the deposition of continuous strain-gauge resistors.
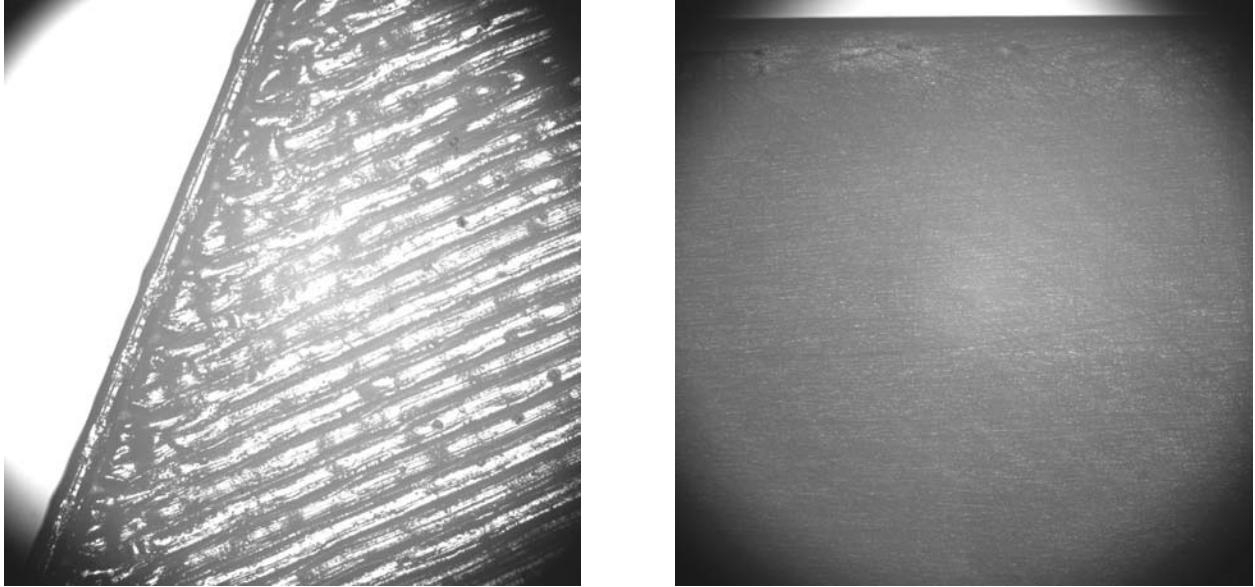
Figure 11: ABS plastic surface before (left) and after (right) polishing.

References

[1] V. I. Fernandez, S.M. Hou, F. S. Hover, J. H. Lang and M. S. Triantafyllou; "MEMS-Array Pressure Sensing for Underwater Navigation"; *Proceedings: 2007 Undersea Distributed Networked Systems Conference*; Newport, RI, February 2007.

[2] V. I. Fernandez, S. M. Hou, F. S. Hover, J. H. Lang and M. S. Triantafyllou; "Lateral-line inspired MEMS-array pressure sensing for passive underwater navigation"; *Proceedings: Unmanned Untethered Submersible Technology Symposium*; Durham, NH, August 2007.

[3] T Suzuki and T Colonius; "Inverse-imaging method for detection of a vortex in a channel"; *AIAA Journal*, 41:9, 1743-1751, 2003.